doi:10.1016/j.jmb.2006.03.010 J. Mol. Biol. (2006) 358, 1314–1327

JMB

Available online at www.sciencedirect.com

SCIENCE DIRECT®

ELSEVIER

Desulfovibrio desulfuricans G20 Tetraheme Cytochrome Structure at 1.5 Å and Cytochrome Interaction with Metal Complexes

M. V. Pattarkine[1], J. J. Tanner[1,2], C. A. Bottoms[3], Y.-H. Lee[4] and J. D. Wall[1]*

[1]*Biochemistry Department University of Missouri-Columbia Columbia, MO 65211, USA*

[2]*Chemistry Department University of Missouri-Columbia, Columbia, MO 65211 USA*

[3]*Health Management & Informatics, University of Missouri-Columbia, Columbia MO 65211, USA*

[4]*Structural Biology Core University of Missouri-Columbia, Columbia, MO 65211 USA*

**Corresponding author*

The structure of the type I tetraheme cytochrome c_3 from *Desulfovibrio desulfuricans* G20 was determined to 1.5 Å by X-ray crystallography. In addition to the oxidized form, the structure of the molybdate-bound form of the protein was determined from oxidized crystals soaked in sodium molybdate. Only small structural shifts were obtained with metal binding, consistent with the remarkable structural stability of this protein. *In vitro* experiments with pure cytochrome showed that molybdate could oxidize the reduced cytochrome, although not as rapidly as U(VI) present as uranyl acetate. Alterations in the overall conformation and thermostability of the metal-oxidized protein were investigated by circular dichroism studies. Again, only small changes in protein structure were documented. The location of the molybdate ion near heme IV in the crystal structure suggested heme IV as the site of electron exit from the reduced cytochrome and implicated Lys14 and Lys56 in binding. Analysis of structurally conserved water molecules in type I cytochrome c_3 crystal structures identified interactions predicted to be important for protein stability and possibly for intramolecular electron transfer among heme molecules.

Keywords: *Desulfovibrio*; tetraheme cytochrome c_3; metal reduction; X-ray crystallography; bioremediation

Introduction

Sulfate-reducing bacteria of the genus *Desulfovibrio* are anaerobes that derive energy from the dissimilatory reduction of sulfate with the oxidation of dihydrogen or organic substrates. Additionally, these bacteria enzymatically reduce toxic metals such as chromium (VI), manganese (IV), iron (III),[1] technetium (VII),[2] and uranium (VI).[3] However, metal reduction has not been demonstrated to support growth with any consistency. When uranium is reduced, the soluble U(VI) is converted to U(IV), which precipitates as the insoluble mineral uraninite, UO_2. Currently, this metabolism is being explored for its potential application to bioremediation of groundwater contaminated with uranium.[4]

The tetraheme cytochrome c_3 is a periplasmic redox protein from Gram-negative sulfate-reducing bacteria.[5] As their most abundant *c*-type cytochrome, it has been implicated in the transfer of electrons and protons from periplasmic hydrogenases[6,7] and other periplasmic dehydrogenases to the electron transfer chain for sulfate respiration and ATP synthesis, respectively. The role of the *Desulfovibrio* cytochrome c_3 in uranium reduction has been investigated *in vitro* through spectroscopic studies and by pathway reconstitution experiments.[8] The results of these studies supported a model of electron flow from hydrogen through hydrogenase to cytochrome c_3 to U(VI). While recent evidence from mutant analyses confirmed that cytochrome c_3 was a part of the *in vivo* electron transfer pathway to U(VI) from hydrogen, evidence was found for alternative pathways from organic donors that could bypass this tetraheme cytochrome.[9]

This small (~13,000 Da) soluble *c*-type cytochrome has four heme molecules with bis-histidinyl axial

Present address: Y.-H. Lee, Department of Biological Sciences, Louisiana State University, 202 Life Sciences Bldg, Baton Rouge, LA 70803, USA.

Abbreviations used: CD, circular dichroism; RMSD, root-mean-square difference.

E-mail address of the corresponding author: wallj@missouri.edu

ligation.[5] Because it is encoded by a monocistronic gene, has CXXCH and CXXXXCH heme-binding motifs, and has the characteristic conserved lysine residues, it is classified as type I cytochrome c_3 (TpI-c_3).[10–12] The adjacent pairs of heme planes are almost perpendicular to each other and are oriented by a minimum of protein matrix.[5] The different redox potentials of the four heme molecules have been shown to be modulated by several factors, such as the nature of the axial ligands, solvent accessibility and interaction of the porphyrin ring substituents with the neighboring amino acid residues.[5,13–15] To reach an understanding of the mechanism of electron transfer by cytochrome c_3 at the molecular level, knowledge of the architecture of the heme pockets is a critical requirement. High-resolution X-ray structure data for the oxidized tetraheme cytochrome c_3 from five different species of *Desulfovibrio* and one from *Desulfomicrobium*[16–21] have revealed key amino acid residues that are likely to be critical for electron transfer. NMR studies support the correctness of these structures and have been used to elucidate the solution structure of the reduced protein.[22–25] The three-dimensional structures of cytochromes c_3 from these species show highly conserved architecture for the heme core, despite very low levels of sequence homology.[5,20] This diversity in sequence generates different environmental conditions around each heme, resulting in a range of redox potentials, pH-dependence and rates of electron transfer.[5,22]

Positive cooperativity during reduction of cytochromes c_3 has been demonstrated and suggested to be a mechanism for simultaneous multi-electron capture.[7,12] In addition, heterotropic cooperativity or redox Bohr effects have been documented that show thermodynamic linkage between reduction and protonation.[12,23] It has been suggested that this linkage allows charge separation in the absence of a membrane.[7] Because of its dual activities and the limited occurrence of this cytochrome in prokaryotes outside of the δ-Proteobacteria, it may play a critical role in the metabolism of these bacteria.

The specificity of intermolecular electron transfer is provided by molecular recognition. Cytochrome c_3 interacts effectively with a large array of electron-transfer proteins, including hydrogenases,[6,26] a unique high molecular mass cytochrome *c* (Hmc),[27] ferredoxins,[28] flavodoxins,[29] rubredoxin,[29] and a large inorganic polyanion.[30] Several of these successful interactions are unlikely to have physiological meaning, since the proteins occur in different cellular compartments; however, information about the sites of potential electron transfer into and out of cytochrome c_3 has been gained from these studies. In most cases, *in silico* docking of crystal structures of proteins and NMR chemical shift perturbations point to heme IV (the heme numbering convention used is as the binding site occurs in the amino acid sequence) as the site of protein–protein interactions for electron transfer.[26,31] The broad range of substrates would suggest that specificity of the interactions is low and that general features of the protein, such as surface charges allowing electrostatic interactions, may dominate the docking that facilitates electron transfer.

In order to understand the role of cytochrome c_3 in energy transduction as well as enzymatic metal reduction, the interplay of various molecular influences on redox state and heme–heme interactions involved in the process must be elucidated. High-resolution structures of cytochrome c_3 coupled with spectral studies of this redox active protein may provide information about the molecular mechanism involved. Here, we describe the crystal structure of the oxidized cytochrome c_3 from *Desulfovibrio desulfuricans* strain G20 (G20c_3) at 1.5 Å resolution. The structure of the oxidized protein bound to the molybdate ion revealed a binding site near heme IV, in agreement with the inference that this site effectively interacts with substrates.[26,31] Binding of molybdate caused no large protein rearrangement. The crystal structures were complemented with functional studies of Mo(VI) and U(VI) oxidation of reduced G20c_3. These studies provide the foundation for the elucidation of the specific amino acid residues of G20c_3 essential for metal interaction and for normal physiological function of cytochrome c_3 in these bacteria. Finally, we examined the conservation of protein-bound water in available crystal structures of the TpI-c_3 family. Several highly conserved water molecules are likely important for overall protein structure and stability, while a pocket of water molecules at the intersection of heme I, heme II, and heme III may be involved in electron transfer among the heme molecules.

Results and Discussion

UV-Vis spectroscopy measurements

To determine whether efficient electron transfer could occur from reduced purified G20c_3 to the uranyl ion, the changes in UV-visible light absorption by G20c_3 following reduction and metal exposure to the reduced G20c_3 were monitored. The absorption spectrum of as-isolated oxidized G20c_3, dithionite-reduced and G20c_3 oxidized following addition of uranyl acetate are shown in Figure 1. The addition of U(VI) as the uranyl ion clearly oxidized the reduced G20c_3 and the spectrum of this metal-oxidized protein resembled that obtained for the as-isolated air-oxidized protein (spectrum 4 *versus* 1). The amount of U(VI) necessary for apparent complete protein oxidation was near the theoretical stoichiometry of 2:1.

The Soret peak of the U(VI)-oxidized protein at 408 nm was consistently decreased about 5–8% in absorbance with respect to that expected for the amount of G20c_3 present. The cause of this decrease was not apparent, although G20c_3 binding to insoluble metal oxides has been documented.[32] When subjected to three sequential cycles of reduction and metal addition, the shapes of the spectra were identical, although the absorbance at

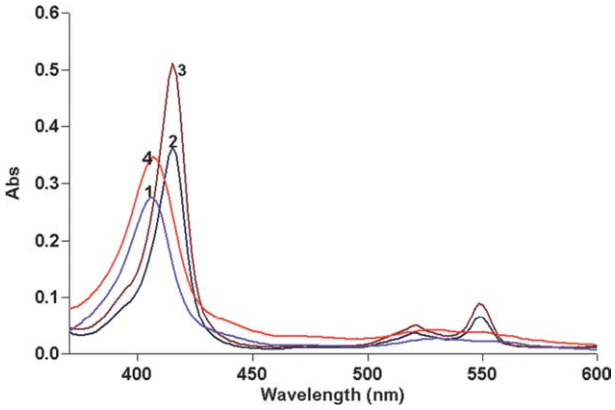

Figure 1. UV-Vis spectra of oxidized, reduced and U(VI) oxidized G20c_3 in 10 mM Tris–HCl (pH 7.6). Spectra were made of the following: (1) 1.4 μM oxidized G20c_3; (2) 1.4 μM G20c_3 and 50 μM sodium dithionite; (3) 2.0 μM G20c_3 (the increase is from titration of excess dithionite) and 50 μM sodium dithionite; (4) 2.0 μM G20c_3, 50 μM sodium dithionite, and 4 μM uranyl acetate.

408 nm was slightly decreased after each metal oxidation. From this result, it was inferred that the U(VI)-oxidized form resembled the as-isolated G20c_3 structurally and functionally. Oxidation of the protein following U(VI) addition occurred too rapidly to obtain kinetics by standard spectrophotometric procedures.

Spectra were recorded upon addition of sodium molybdate. Work with the triheme cytochrome c_7 from *Desulfuromonas acetoxidans* establishing the reduction of chromium (VI) to chromium (III) used the molybdate ion to identify the binding site for the chromate ion.[33] Even though the molybdate ion was not redox active under the conditions used, it was chosen for being isostructural and isoelectronic with chromate. Cytochrome c_7 shares structural homology and the ability to reduce chromate with other tetraheme *c*-type cytochromes,[34] making the results with that protein relevant to the family of tetraheme cytochromes. While MoO_4^{2-} is neither isostructural nor isoelectronic with UO_2^{2+}, it was the first model of a metal substrate for which the binding site was located on a cytochrome in this family.[33] When a 2 μM solution of reduced G20c_3 was made 30 μM in MoO_4^{2-}, remarkably, the protein was oxidized and the spectrum of the resulting protein was essentially identical with that obtained with the addition of U(VI) (data not shown). As compared with the concentration of uranyl ion needed for complete oxidation of the reduced cytochrome, approximately 7.5-fold more MoO_4^{2-} was required.

Circular dichroism studies

To explore possible G20c_3 structural perturbations accompanying oxidation and reduction, and those that might occur through the interaction of oxidizing metals, circular dichroism (CD) spectra were recorded. The CD spectra of proteins in the chromophoric and peptide regions sensitively reveal alterations in structure.[35,36] In the case of oxidized G20c_3, the CD in the Soret region indicated a slight asymmetry in the vicinity of the hemes; whereas, in the far-UV region, the overall secondary structure of the protein appeared to be dominated by α-helical structure. These results were quite similar to those reported for other tetraheme cytochromes.[37] The CD spectra for the oxidized, reduced, and U(VI)-oxidized G20c_3 are shown in Figure 2.

Upon reduction, a negative peak appeared at 425 nm in the Soret region, and the positive maximum shifted from 408 nm to 418 nm. This red shift of the Soret peak parallels the changes seen in the UV-visible absorption spectrum upon reduction of G20c_3, indicating the absence of any major conformational perturbations of the heme chromophore linked to oxidation-reduction.[36] Oxidation of the reduced protein with U(VI) resulted in a further skew of the Soret peak that suggested a minor perturbation of the heme environment.

In the far UV, there was a small increase in the ellipticity of the 222 nm band upon reduction. The large dipole of the extended π system of hemes and changes in the heme orientations may produce an alteration of the far-UV CD bands of heme proteins.[35] This interpretation gains support from our X-ray structure data (below) that revealed small, localized changes in the vicinity of heme molecules upon reduction. The U(VI)-oxidized G20c_3 sample also exhibited slight changes in the far UV that reflected interactions with heme molecules or minor perturbations of α-helix structure. Controls of oxidized G20c_3 in the presence of identical amounts of uranyl acetate exhibited no detectable change when compared to spectra of oxidized protein alone (data not shown).

The CD spectrum of the MoO_4^{2-} -oxidized G20c_3 was not different from that of the U(VI)-oxidized form (data not shown), except that the Soret band of

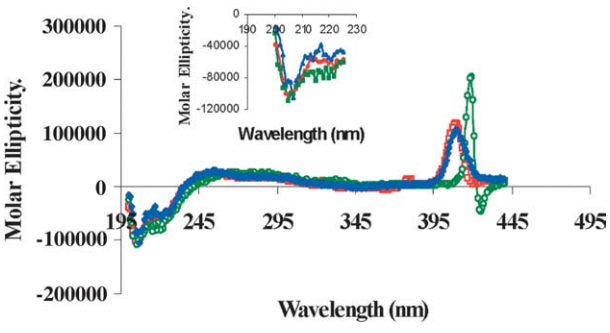

Figure 2. Circular dichroism spectra of oxidized, reduced and U(VI)-oxidized G20c_3 in 10 mM phosphate buffer (pH 7.6). Red spectrum, 2 μM G20c_3; green spectrum, 2 μM G20c_3, 50 μM sodium dithionite; blue spectrum, 2 μM G20c_3, 50 μM sodium dithionite, 4 μM uranyl acetate. Typical spectra of at least eight trials. Inset: an expanded view of far-UV scans.

the metal-oxidized protein was 10–15% decreased from that of the initial oxidized G20c_3, as compared to the 5–8% found for U(VI)-oxidized protein. This decrease might result from the higher concentration of metal needed for oxidation of the protein.

To determine the relative thermal stability of the air-oxidized and the U(VI)-oxidized forms of G20c_3, we conducted thermal melting experiments with both samples monitored at 206 nm, a wavelength where α-helical structure changes would be detected. The thermal melting profiles for both forms of G20c_3 were essentially identical (data not shown), indicating that metal interaction did not alter the native structure sufficiently to cause significant changes in the thermostability of G20c_3.

The melting temperatures (T_m)[38] of the as-isolated oxidized and U(VI)-oxidized proteins were 108 °C and 110 °C, respectively, within the error range (4 °C) of the technique. These proteins showed no spectral differences upon two rounds of heating to 105 °C and cooling to 25 °C. These data confirmed the exceptional thermal stability found for cytochromes c[39] and c_3,[37] and indicated that U(VI)-oxidized protein was structurally and functionally similar to the as-isolated oxidized G20c_3.

Stopped-flow kinetics studies

Since the rate of oxidation of reduced G20c_3 by uranyl acetate was quite rapid, the redox reaction was monitored by stopped-flow absorbance measurements at the α absorption band of G20c_3, A_{553} (Figure 3). The observed rate constant for G20c_3 oxidation exhibited a hyperbolic dependence on the concentration of uranyl acetate, indicating a two-step binding and oxidation mechanism.[40] Although the transients at higher concentrations of uranyl acetate appeared to fit better to a double exponential, there was no consistent concentration-dependence for the second rate constant. Therefore the data were analyzed by fitting to a single exponential at all concentrations. Equation (1) was

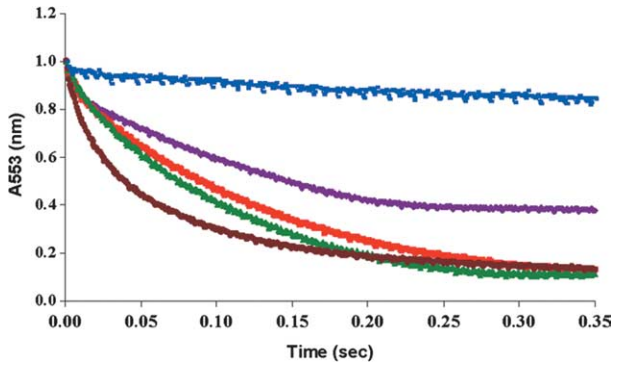

Figure 3. Fast kinetics of G20c_3 oxidation by uranyl acetate in 10 mM phosphate buffer (pH 7.6). Concentration of reduced G20c_3, 2 μM. Concentrations of uranyl acetate: blue, zero (buffer alone control); purple, 20 μM; red, 30 μM; green, 50 μM; and brown, 150 μM. The temperature was 22 °C.

Table 1. Kinetic parameters for oxidation of *Desulfovibrio desulfuricans* G20 cytochrome c_3 with uranyl acetate or sodium molybdate

Oxidant	K_1 (μM^{-1})	k_2 (s^{-1})	k_{-2} (s^{-1})
Uranyl acetate	0.017±0.003	34.1±1.3	0.4±1.5
Sodium molybdate	0.008±0.003	0.96±0.08	3.2±0.1

used to fit the data, which yields values for K_1, the association constant between uranyl acetate and G20c_3, k_2, the forward rate constant for oxidation of G20c_3 from the protein–uranyl acetate complex, and k_{-2}, the rate constant for the reverse reaction (Table 1).

$$\lambda = K_1 k_2 [S]/(K_1[S] + 1) + k_{-2} \quad (1)$$

Analysis yielded a value of $1.7\times10^8\ M^{-1}$ for the association constant, K_1, for uranyl acetate. Similar experiments were performed for MoO_4^{2-} oxidation of reduced cytochrome and an association constant of $0.8\times10^8\ M^{-1}$ was obtained. From these results, the uranyl ion seems more effective in interacting with reduced G20c_3 protein than the molybdate ion. Additional studies of ionic strength and buffer pH effects on the rates of G20c_3 oxidation are underway in an attempt to evaluate intermolecular electron transfer further.

Overall structure of G20c_3 and comparison to DvHc_3

The structure of oxidized G20c_3 was determined to 1.5 Å resolution using the molecular replacement method (Table 2). In addition, a 2.3 Å resolution structure of G20c_3 with bound molybdate ion was obtained from a crystal soaked in 10 mM Na_2MoO_4. For both structures, the electron density was continuous for the entire backbone between Ala1 and Pro107, and density representing the four covalently bound porphyrin heme groups was quite strong except for a few of the propionate carboxyl groups. All side-chains were modeled except for three solvent-exposed lysine residues (Lys 9, Lys14, and Lys57), which were presumably disordered. The excellent quality of the 1.5 Å diffraction data collected from the oxidized crystal allowed modeling of alternative side-chain conformations in residues Glu2, Ser23 and Ser25. All three structures exhibit good geometry with no residue in the disallowed region of the Ramachandran plot (Table 2). Note that the average *B*-factor of the molybdate-bound structure is approximately twice that of the oxidized structure. We suspect that the increase in *B*-factor reflects a decrease in crystal quality caused by soaking in Na_2MoO_4.

The structures reported here display the strongly conserved type I tetraheme cytochrome c_3 fold,[19,23,41] which typically consists of a two-stranded anti-parallel β-sheet located in the N terminus of the protein followed by three to five

Table 2. Diffraction data collection and refinement statistics

	Oxidized	Molybdate
PDB accession code	2A3M	2A3P
Wavelength (Å)	0.97856	1.5418
Space group	$P2_12_12_1$	$P2_12_12_1$
Unit cell dimensions		
a (Å)	43.67	43.16
b (Å)	43.88	43.70
c (Å)	57.73	57.89
Diffraction resolution (Å)	35–1.50	27–2.30
Outer shell (Å)	1.55–1.50	2.36–2.30
No. observations	116,721	26,792
No. unique reflections	18,098	5167
Redundancy	6.4 (4.6)	5.2 (5.3)
Completeness (%)	98 (86)	97 (95)
Mean I/σ_I	28.3 (4.1)	16.6 (2.4)
R_{merge}	0.060 (0.238)	0.093 (0.428)
No. protein residues	107	107
No. water molecules	77	9
R_{cryst}	0.175 (0.179)	0.191 (0.215)
R_{free}[a]	0.195 (0.246)	0.248 (0.309)
Coordinate error (Å)	0.04	0.19
RMSD Bond lengths (Å)[b]	0.012	0.012
RMSD bond angles (deg.)[b]	1.2	1.9
Ramachandran plot[c]		
Favored (no. residues)	84	84
Allowed (no. residues)	12	12
Generous (no. residues)	1	1
Disallowed (no. residues)	0	0
Average *B*-factors (Å^2)		
Protein	17	38
Heme	15	36
Water	22	27
Molybdate ion		41

Values for the outer resolution shell of data are given in parentheses.
[a] 10% R_{free} test set.
[b] Compared to the Engh and Huber force field.[63]
[c] The Ramachandran plot was generated with PROCHECK and includes only non-Gly and non-Pro residues.[64]

α-helices. The two strands of G20c_3 are formed by residues 7–10 and 17–19, and there are five α-helices formed by residues 22–24, 29–32, 64–69, 79–87 and 91–98. The closest structural homologue to G20c_3, based on a search of the Protein Data Bank using SSM,[42] is DvHc_3 (PDB code 2CTH). This result is not surprising, because DvHc_3 and G20c_3 share 65% amino acid sequence identity and the DvHc_3 structure was used for molecular replacement calculations. The overall root-mean-square difference (RMSD) between the C^α atoms of the 1.5 Å resolution G20c_3 structure and the DvHc_3 structure is quite low (0.85 Å), and the inter-heme distances and angles of the two structures are comparable (Table 3).

Despite a high level of global structural similarity between G20c_3 and DvHc_3, there are significant local conformational differences in two regions of the polypeptide chain (Figure 4). The first region involves residues 37–41. These residues are on the surface of the protein and the positions of analogous C^α atoms in the two structures differ by as much as 2.8 Å. We speculate that this conformational difference might be due to a non-conservative sequence variation at position 42, which is Leu42 in G20c_3 and Tyr43 in DvHc_3. The hydroxyl group of Tyr43 forms a hydrogen bond with the carboxylate group of Glu41, which pulls these two residues close together in the DvHc_3 structure. An analogous interaction is not possible in the G20 protein, due to the presence of Leu at position 42 and thus residues 40 and 42 in G20c_3 are farther apart than those in DvHc_3.

The second region of structural difference between G20c_3 and DvHc_3 that is potentially more interesting occurs in the loop that separates the 60s helix from the 80s helix (Figure 4), where backbone differences of 3.7 Å were observed. This structural

Table 3. Characteristics of cytochrome c_3 isolated from *D. desulfuricans* G20 compared with that from *D. vulgaris* Hildenborough

Ligands				Edge-to edge distance (Å)			Fe–Fe distance (Å)		Angles between heme planes (°)	
Heme	Residue	G20c_3[a]	DvHc_3[b]	**Heme**	G20c_3	DvHc_3	G20c_3	DvHc_3	G20c_3	DvHc_3
I	Cys	29	30	**I-II**	6.3	6.4–6.6	12.3	12.2–12.4	90–92	88–90
	Cys	32	33	**I-III**	6.1	5.8–6.0	11.0	11.0–11.2	93–100	81–82
	His	33	34	**I-IV**	9.6	9.7–9.9	17.7	17.7–18.0	19–21	19–22
	His	21	22							
II	Cys	45	46	**II-III**	8.8	8.5–8.8	16.3	15.8–16.1	55	60
	Cys	50	51	**II-IV**	10.8	10.2–10.3	16.9	16.4–16.7	70–74	71–75
	His	51	52							
	His	34	35	**III-IV**	5.5	5.4–5.5	12.2	11.9–12.0	86	80–82
III	Cys	79	79							
	Cys	82	82							
	His	83	83							
	His	24	25							
IV	Cys	100	100							
	Cys	105	105							
	His	106	106							
	His	69	70							

Data for *D. vulgaris* taken from Coutinho & Xavier.[5]
[a] G20c_3 is the type I cytochrome c_3 from *D. desulfuricans* G20.
[b] DvHc_3 is the type I cytochrome c_3 from *D. vulgaris*.

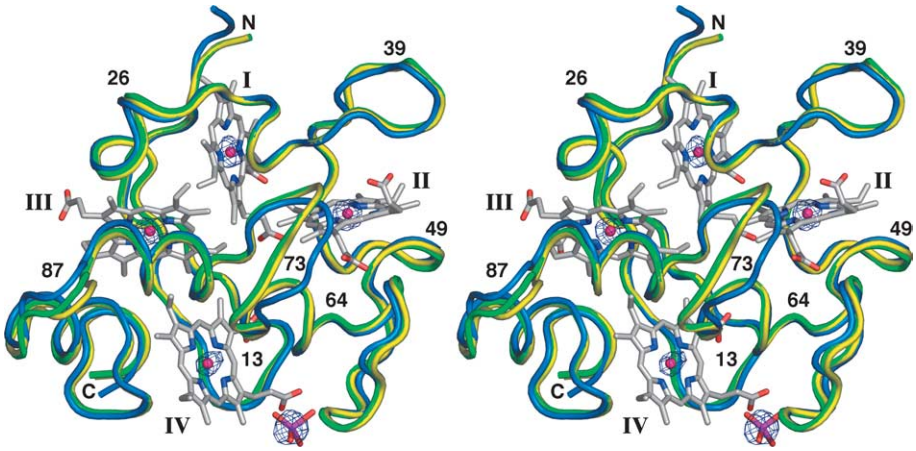

Figure 4. Stereoscopic view of cytochrome c_3 structures from *Desulfovibrio desulfuricans* G20 and *Desulfovibrio vulgaris* Hildenborough (PDB code 2CTH). The oxidized and molybdate-bound forms of *D. desulfuricans* c_3 are colored green and yellow, respectively. The structure of *D. vulgaris* Hildenborough c_3 is shown in blue. The heme molecules and the molybdate ion of the molybdate-bound c_3 structure are drawn in ball-and-stick mode. The heme molecules are labeled with roman numerals. The electron density map (3 σ) is an anomalous difference Fourier map calculated from the molybdate data set. Note the strong electron density feature covering the molybdate ion, which is bound to heme IV.

difference is most likely caused by two sequence variations. First, there is an insertion of one residue (Arg71) in the G20 sequence, which increases the length of the loop in G20c_3. Second, Thr75 in G20c_3 replaces Lys75 in DvHc_3. This sequence variation is highly significant, because Lys75 forms an ion pair with a propionate group of heme II in DvHc_3 (Figure 5). This interaction, possibly in combination with the sequence difference at position 73, draws the loop close to heme II in DvHc_3. In contrast, the Thr side-chain at position 75 in the G20 protein is too short to interact with heme II. The observed structural variation suggests that there is a tighter coupling between hemes II and IV in DvHc_3 than in G20c_3.

Molybdate-bound G20c_3 structure

Binding of molybdate caused no significant changes to the global protein structure (Figure 4). The RMSD values between the oxidized and molybdate-bound structures were small: 0.22 Å for C^{α} atoms and 0.47 Å for all atoms. These results agree with previous reports for cytochromes,[43] in which only small changes in structure were documented upon ligand binding or reduction.

Although the binding of molybdate did not cause significant protein structural changes, three heme propionate groups have been modeled in different conformations in the G20c_3 structures (propionate A of hemes I and II, propionate D of heme III). However, it was difficult to assess whether molybdate-binding directly caused these changes, because the electron density representing the carboxyl moieties of these particular propionate groups was rather weak. The apparent differences in conformation could simply reflect a natural flexibility of these regions of the heme molecules and thus the significance of these apparent conformational changes was unclear.

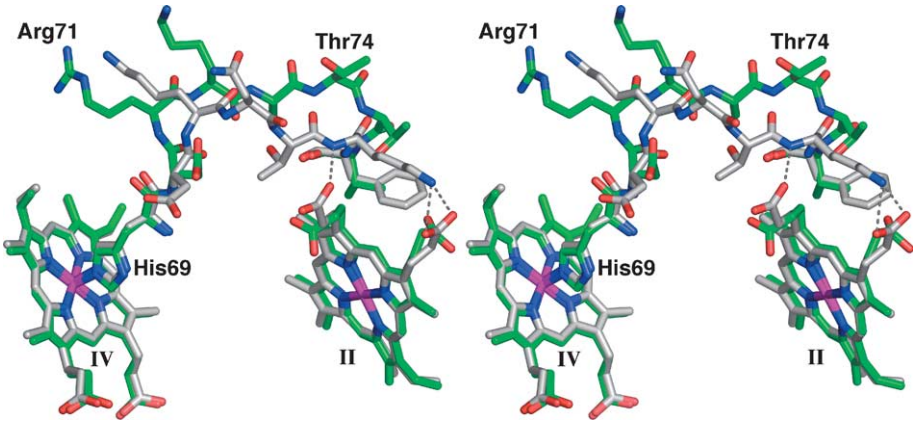

Figure 5. Stereoscopic view of cytochrome c_3 structures from *Desulfovibrio desulfuricans* G20 and *Desulfovibrio vulgaris* Hildenborough (PDB code 2CTH) highlighting structural differences in residues 69–75. The oxidized structure of *D. desulfuricans* c_3 is shown in green. The *D. vulgaris* Hildenborough c_3 structure is shown in white. The residue numbering corresponds to *D. desulfuricans* c_3. Dotted lines indicate electrostatic interactions within a cutoff distance of 3.2 Å.

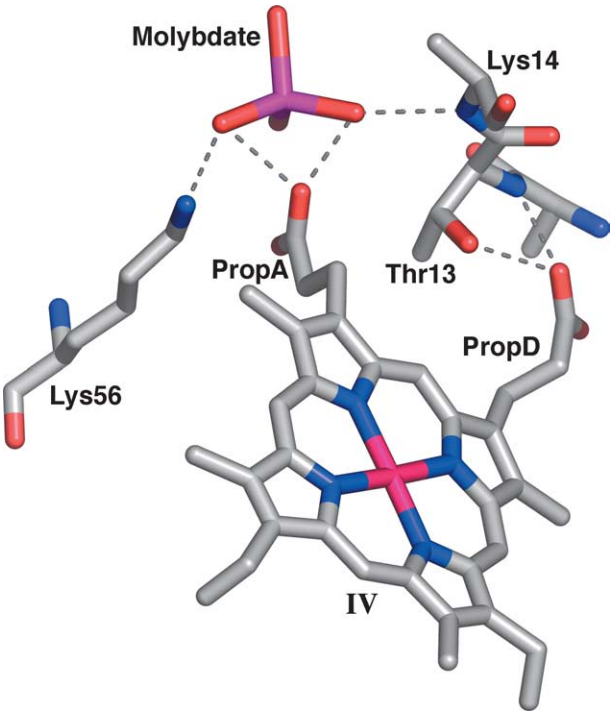

Figure 6. Molybdate-binding site of *Desulfovibrio desulfuricans* G20 cytochrome c_3. Dotted lines indicate electrostatic interactions within a cutoff distance of 3.2 Å.

Anomalous difference Fourier analysis using data collected from an oxidized crystal soaked in 10 mM Na_2MoO_4 revealed the presence of a strong anomalous scattering center located near propionate A of heme IV (Figure 4). On the basis of this evidence, a molybdate ion was modeled in this site. The average *B*-value for molybdate refined to 41 Å^2, which is comparable to the *B*-values for the protein (38 Å^2) and heme molecules (36 Å^2). Thus, the molybdate ion bound to the protein with high occupancy.

G20c_3 interacts with the bound molybdate through an ion pair to Lys56 and a hydrogen bond with the backbone amine group of Lys14 (Figure 6). These interactions bring the Mo atom within 2.4 Å of an oxygen atom of heme IV propionate A. Because molybdate was found to function as an electron acceptor from dithionite-reduced G20c_3, and preliminary data from a site-directed mutant K14A of G20c_3 showed that molybdate could no longer oxidize this mutant protein (S. Miller & J.D.W., unpublished results), we infer that heme IV may be the primary site of electron exit from the protein, in agreement with other results.[12,20,41,44] Moreover, we predict that Lys56 is essential for reduction of molybdate, and possibly uranyl acetate, by G20c_3. This prediction will be tested by mutagenesis studies.

Structurally conserved solvent sites

Acquisition of a new high-resolution TpI-c_3 structure prompted us to analyze structural conservation of protein-bound water molecules in this protein family. Our analysis revealed 11 solvent sites with 100% conservation in the TpI-c_3 family (Table 4; Figure 7). Most of the conserved protein–water interactions involve the protein backbone; however, there are also conserved hydrogen bonds with three of the heme-coordinating His side-chains (sites 1–3, Table 4) and a propionate group of heme I (site 9, Table 4).

Site 1 has been discussed by Aragao *et al.* as possibly facilitating electron transfer between hemes I and II.[45] This water molecule forms hydrogen bonds with the imidazole group of His33 (G20c_3 numbering) and the main-chain carbonyl group of Ala43 (G20c_3 numbering) in all of the structures that we studied (Table 4; Figure 8(a)). Note that His33 is a coordinating ligand of the Fe bound to heme I. In addition, 67% of the structures had a hydrogen bond between site 1 and a backbone carbonyl group (Asn41 in G20c_3). This water molecule is present in both of our structures (HOH 4) and has *B*-values of 10–26 Å^2.

We also discovered ten novel conserved solvent sites (Table 4), which have not been discussed previously as globally conserved in the TpI-c_3 family. For example, site 2 is related to site 1 by approximate mirror symmetry through the plane of heme I (Figure 8(a)). As with site 1, water molecules in site 2 form hydrogen bonds with an Fe-coordinating imidazole group (His21 in G20c_3) and two backbone carbonyl groups. In addition, site 2 water molecules form a hydrogen bond with the backbone amine group of His21. Thus, the coordination environment of site 2 provides the full complement of two hydrogen bond donors and two hydrogen bond acceptors. Accordingly, this water molecule has a rather low *B*-value in our structures, ranging from 9 Å^2 in the oxidized structure to 24 Å^2 in the molybdate-bound structure.

Table 4. Solvent sites of the type I tetraheme cytochrome c_3 family that were 100% conserved in reported structures

		Representative interactions	
Site	Water ID	Backbone (%)	Side-chain (%)
1	4	O-Asn41 (67) O-Ala43 (100)	ND1-His33 (100)
2	1	O-Ala5 (100) O-Phe19 (100) N-His21 (100)	ND1-His21 (100)
3	46	O-Pro16 (67)	ND1-His106 (100)
4	14	O-Val53 (100) O-Asp55 (83) N-Tyr65 (100)	
5	10	N-Ile18 (100) O-Cys105 (100)	
6	8	O-Tyr27 (100)	
7	23	O-His21 (100)	
8	53	O-Leu84 (100) O-Gly88 (67)	
9	9	N-Ala46 (100)	PropD-heme I (100)
10	22	N-Lys44 (100)	
11	41	N-Leu42 (100)	

Water ID and representative interactions were obtained from PDB accession code 2A3M.

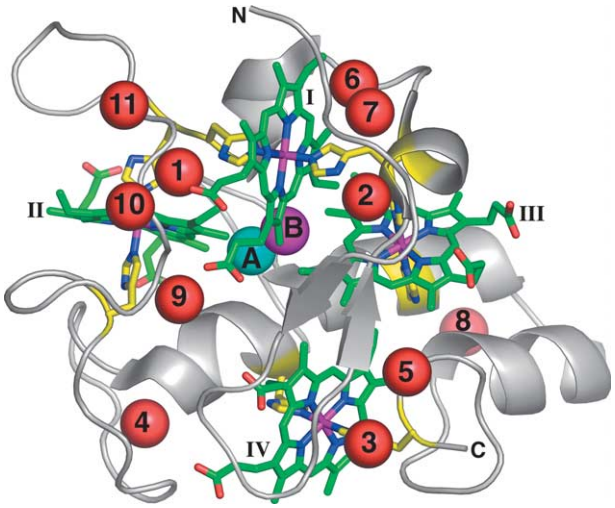

Figure 7. Global structural context of conserved solvent sites of the TpI-c_3 family. The G20c_3 structure is shown as a ribbon drawing, with heme molecules in green and Fe-coordinating His side-chains in yellow. Red spheres represent the 11 100% conserved solvent sites of the TpI-c_3 family, with numbers corresponding to the site numbers given in the left-most column of Table 4. Water molecules in the conserved solvent-filled pocket are represented by the cyan (cluster A) and magenta (cluster B) spheres.

As with sites 1 and 2, conserved site 3 interacts with a histidinyl heme ligand (Figure 8(b)). Water molecules bound to site 3 form hydrogen bonds with a His side-chain bound to heme IV Fe (100% conserved) and a backbone carbonyl group (67% conserved). Thus, three of the eight heme-coordinating imidazole groups engage in hydrogen bonds with conserved water molecules in TpI-c_3 (for example, His21, His33, and His106 in G20c_3). Presumably, the conserved His–solvent hydrogen bonds formed by water molecules in sites 1–3 help stabilize and orient the heme-binding site by non-covalently linking the imidazole/heme unit to the protein backbone. We note that the other five Fe-coordinating His side-chains of TpI-c_3 form hydrogen bonds with backbone carbonyl groups, rather than with conserved water molecules. Thus, consideration of conserved solvent structure leads to the observation that the hydrogen bonding potential of the heme-coordinating imidazole groups in TpI-c_3 is fully satisfied. To our knowledge, this aspect of c_3 structure has not been described previously.

Sites 1 and 4 are noteworthy because conservation of these solvent sites extends beyond the TpI-c_3 family to type II cytochrome c_3 (TpII-c_3) and cytochrome cc_3 proteins. Examples of these proteins for which structures are known include TpII-c_3 from

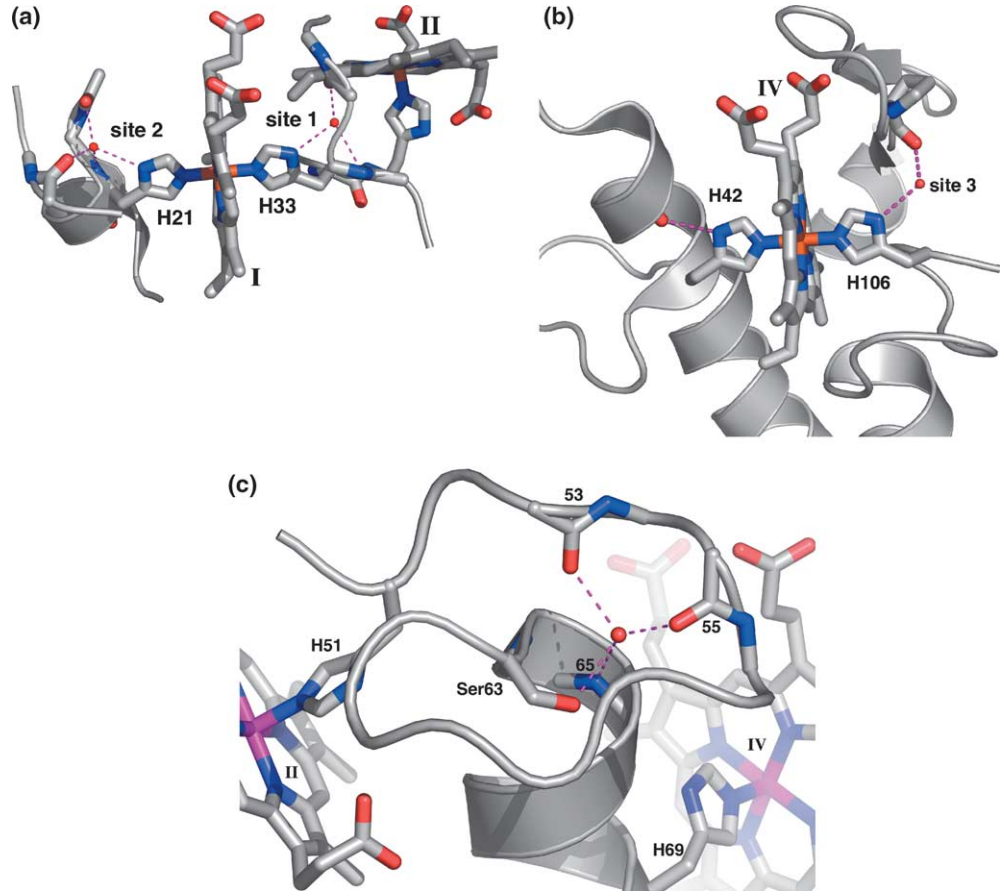

Figure 8. Close-up views of conserved solvent sites 1–4. (a) Conserved solvent sites 1 and 2 from the 1.5 Å resolution G20c_3 structure. Broken lines denote hydrogen bonds. (b) Conserved solvent site 3 from the G20c_3 structure. (c) Conserved solvent site 4 from G20c_3.

Desulfovibrio desulfuricans Norway (2CY3)[17] and *Desulfovibrio africanus* (3CAO),[20] as well as cytochrome cc_3 from *D. desulfuricans* Norway (1AQE)[46] and *Desulfovibrio gigas* (1GYO).[45] The structural features that distinguish TpI-c_3 and TpII-c_3 proteins have been described.[10] Among the more notable differences, TpII-c_3 and cc_3 proteins feature a shorter C-terminal α-helix, which typically consists of only four residues, compared to the seven to ten residue C-terminal α-helix of TpI-c_3 structures. Also, the long loop separating the 60s and 80s α-helices found in TpI-c_3 ("interhelix loop") is more compact in cc_3 (1AQE, 1GYO) and absent from TpII-c_3 (2CY3, 3CAO).

The fact that solvent site 1 is present in all cytochrome c_3 proteins attests to the strength of the protein–water interactions formed by water molecules in this site and provides additional support for this water molecule playing a functional role in electron transfer, as suggested by Aragao *et al.*[45] Unlike site 1, site 4 is not associated with a heme. Rather, site 4 sits atop the N terminus of the 60s helix (Figure 8(c)). The water molecule in this site fills the space between the helix N terminus and the long loop that precedes the 60s helix. This water molecule always forms one or two hydrogen bonds with backbone carbonyl groups of the loop plus a hydrogen bond with a backbone amine of the first or second residue of the helix (Figure 8(c)). In addition, it forms a hydrogen bond with the 60s helix N_{cap} side-chain in G20c_3, 3CYR, 1WAD and 1I77. This water molecule tends to be more buried in TpI-c_3 structures than in the TpII-c_3 structures. In either case, though, the water molecule bound to this site links two secondary structural elements. Conservation of this solvent site in the TpI-c_3, TpII-c_3 and cc_3 families suggests that these water-mediated interactions are important for protein stability and folding.

Conserved solvent-filled pocket

Manual inspection of the TpI-c_3 structures used for the water analysis described above also revealed a conserved solvent-filled pocket located at the intersection of hemes I, II and III (Figure 9(a)). The pocket in G20c_3 is formed by the three aforementioned heme molecules, residues 31–32, 67–68 and 76–79. Note that residues 76–79 are part of the interhelix loop. Water molecules near the bottom of the pocket can be grouped into two clusters, labeled A and B (Figure 9). Cluster A water molecules form hydrogen bonds with a carbonyl group of the 60s helix and/or the amine group of one of the Cys residues bound to heme III. Cluster B water molecules form hydrogen bonds to cluster A water molecules but they do not form hydrogen bonds directly to the protein. All six TpI-c_3 structures in our non-redundant data set have a cluster B water molecule and all but 3CYR have a cluster A water molecule. Water molecules in clusters A and B typically form hydrogen bonds to other water molecules that form a solvent chain leading to the protein surface (Figure 9). Meyer has described similar solvent chains connecting active sites to bulk solvent, and has proposed that these chains may provide a mechanism for proton transport to/from the active site.[47]

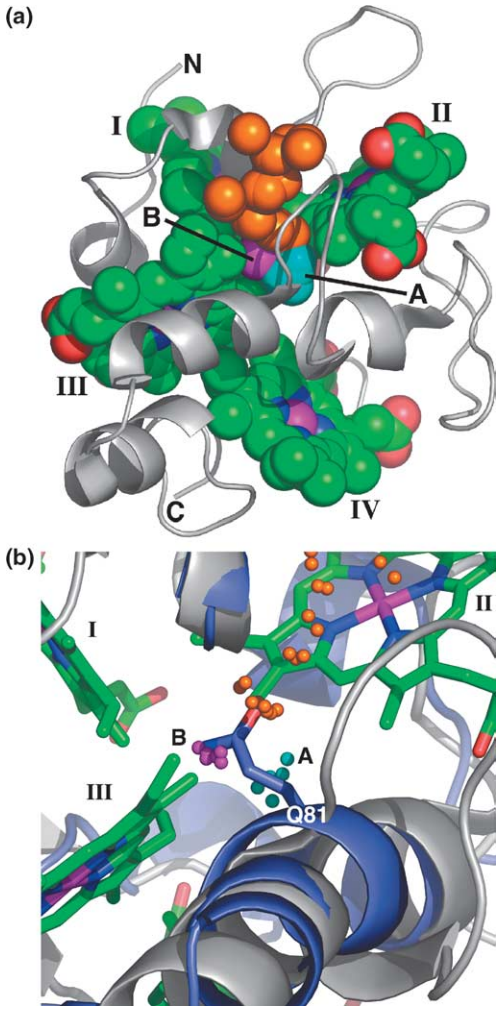

Figure 9. Conserved solvent-filled pocket. (a) Global view of the pocket with G20c_3 polypeptide represented as a ribbon drawing (white) and the heme molecules of G20c_3 shown in CPK mode (green). Water molecules from six superimposed TpI-c_3 structures are shown as cyan (cluster A) and magenta (cluster B) CPK spheres. Orange spheres represent water molecules from the six structures that form a chain leading from the pocket to the protein surface. (b) Close-up view of the conserved, solvent-filled pocket. The coloring scheme is the same as in (a), except that water molecules of the six TpI-c_3 structures are drawn as small spheres, heme molecules of G20c_3 are drawn as sticks and the TpII-c_3 structure 3CAO is shown in blue. Gln81 of 3CAO is shown. The orientation in (b) is slightly rotated from that in (a).

Interestingly, this pocket is present also in TpII-c_3 and cc_3 structures, but it is not always filled with water. The cc_3 structures 1AQE and 1GYO have a cluster B water molecule in the pocket but no water molecule in cluster A. In these structures, the volume corresponding to cluster A is reduced due

to a shift of heme II 1 Å toward the pocket centroid (relative to G20c_3). On the other hand, TpII-c_3 structures 2CY3 and 3CAO have a Gln side-chain (Gln91 in 2CY3, Gln81 in 3CAO) filling the pocket rather than water molecules (Figure 9(b)). We note that 2CY3 and 3CAO are unique among the structures examined, in that they lack the interhelix loop (Figure 9(b)). Thus, water in the pocket correlates with the presence of the interhelix loop.

Nørager *et al.* observed that reduction of *D. africanus* TpII-c_3 causes rotation of the Gln81 side-chain out of the pocket and subsequent entry of one water molecule into the pocket.[20] On the basis of the location of the pocket at the intersection of three heme molecules and the observation of redox-induced structural changes inside the pocket in one system, we suggest that water molecules in the pocket may have functional significance, perhaps by mediating electron transfer between the cofactors.

Materials and Methods

Bacterial strains

The sulfate-reducing bacterium *D. desulfuricans* strain G20 is a spontaneously nalidixic acid-resistant derivative of the wild-type strain G100A[48] that is also cured of the endogenous cryptic plasmid pBG1.[49]

Isolation and purification of G20c_3

D. desulfuricans strain G20 was grown in 10 l batches on LS medium (medium containing 60 mM sodium lactate and 50 mM sodium sulfate) under anaerobic conditions.[50] Cells were harvested from early stationary phase (A_{600nm} ~ 0.93) by centrifugation (4000*g*, 10 min, 4 °C). The cell pellets were suspended in 200 ml of extraction buffer (50 mM Tris–HCl (pH 9.0), 50 mM EDTA), stirred gently in an ice-bath for 45 min to release periplasmic proteins, and centrifuged (13,000*g*) for 45 min at 4 °C.[51] Interestingly, recent proteomics experiments have shown that cytoplasmic proteins are released along with periplasmic proteins by this procedure;[52] however, we find enrichment for cytochrome c_3 by this step. The supernatant containing G20c_3 was loaded onto a hydroxyapatite column (5 cm × 10 cm) equilibrated with 10 mM Tris–HCl (pH 7.6), and the orange-pink protein band was eluted with a gradient of 0.2 M–0.5 M potassium phosphate buffer (pH 7.6). The peak fractions containing G20c_3 were subsequently dialyzed against 10 mM Tris–HCl (pH 7.6) at 4 °C for 4 h. Generally, this fractionation resulted in 1.5–1.8 mg of protein ~95% pure that migrated as a single band during SDS-PAGE. For Western blot analyses, denaturing polyacrylamide gels were transferred onto a nitrocellulose membrane (Osmonics, Westborough, PA) and the relative amount of G20c_3 present was detected by antiserum raised to purified protein as reported earlier.[50] Detection of heme in the proteins separated by SDS-PAGE was accomplished by the peroxidase activity of hemoproteins.[53] Total protein concentration was determined by Bradford analysis[54] with bovine serum albumin as a standard.

UV-Vis spectroscopy

UV-visible absorption spectroscopy studies used a Cary 1 Bio UV-Visible spectrophotometer at room temperature. Screw-capped sealable quartz cuvettes (Starna Cells Inc., Atascadero, CA) were used to obtain anaerobic conditions. To achieve anaerobiosis, empty cuvettes and gas-tight syringes used for solution transfers were flushed with argon before adding the reactant solutions. The reaction buffer (10 mM Tris–HCl, pH 7.6) was bubbled with argon before use. The volume changes from evaporation during the bubbling were less than 5%. A 100 mM sodium dithionite stock solution was made in anaerobic reaction buffer and used within 2 h. Special care was taken while preparing this reductant solution to minimize differential changes in the effective reducing power due to exposure to oxidizing components. G20c_3 (1 μM) was reduced chemically by addition of a buffered solution of sodium dithionite to a final concentration of 50 μM in 10 mM Tris–HCl (pH 7.6). To consume any effective reductant remaining, a predetermined amount of oxidized G20c_3, usually about 1 μM, was added to the cuvette. The aliquot of oxidized protein to be added was determined by titration of a portion of the same mixture until no further increase of A_{418nm} (the Soret absorption maximum for reduced G20c_3) was observed. Stock solutions of 10 mM uranyl acetate and 20 mM sodium molybdate were prepared in anaerobic reaction buffer and added where indicated. Characteristic absorption spectra of the oxidized, reduced and metal-oxidized G20c_3 were obtained by scanning the samples from 350–600 nm. The molar extinction coefficients calculated for the as-isolated oxidized (λ_{408nm}) and sodium dithionite-reduced G20c_3 (λ_{418nm}) were 188,000 M^{-1} $cm^{-1}$and 248,000 M^{-1} cm^{-1}, respectively.

Circular dichroism spectroscopy

The CD spectra were recorded at 25 °C with an Aviv 62DS spectropolarimeter (Lakewood, NJ) in the region 450–190 nm. Purified G20c_3 at a concentration of 2 μM in 10 mM Tris–HCl (pH 7.6) was used. The spectra of oxidized G20c_3, uranyl acetate, sodium dithionite-reduced G20c_3 or reduced G20c_3 with uranyl acetate or sodium molybdate were recorded. Cuvettes, preparation of solutions, and removal of excess reductant were as described for the UV-visible spectroscopy.

CD melting experiments

To determine the thermostability of the as-isolated oxidized, dithionite-reduced, and metal-oxidized forms of G20c_3, thermal melting experiments were carried out using the spectropolarimeter in the temperature range of 30–110 °C with a temperature step of 2 deg. C. The normalized data for the heating and cooling curves were used to calculate the melting temperatures for the different forms of G20c_3. The melting temperatures of the as-isolated oxidized and uranium-oxidized G20c_3 were calculated using the method of John and Weeks.[38] The experiments were repeated three times to confirm reproducibility of the results.

Fast kinetics studies

The rapid kinetics of oxidation of reduced G20c_3 by anaerobic buffered solutions of uranyl acetate or sodium molybdate were studied using a temperature-controlled

KinTek SF-2000 stopped-flow apparatus (Austin, TX, USA) fitted with a 2.6 cm cell. To eliminate oxygen leaks, the entire system was flushed with argon followed by flushing with buffer de-aerated with argon. Reduction of G20c_3 was carried out in a septum-sealed vial flushed with argon. Sodium dithionite (100 mM stock prepared in anaerobic 10 mM Tris–HCl, pH 7.6) was added to a final concentration of 50 μM to a 1 μM solution of G20c_3 in the same buffer. Excess reductant was removed as described for UV-visible spectroscopy. The reduced G20c_3 was introduced into the fast kinetics apparatus with an Ar-flushed, Hamilton syringe fitted with an air-lock system (Hamilton Co., Reno, NV). The regeneration of oxidized G20c_3 by metals was monitored by changes in absorbance at 553 nm. Appropriate controls for changes in A_{553nm} with buffer alone, sodium molybdate, uranyl acetate or reduced G20c_3 with buffer additions were conducted. Data for each concentration of metal were collected as an average of eight data sets. To obtain the kinetics rate constants, the time-dependent absorbance changes were fit to theoretical curves using KaleidaGraph software, version 3.6 (Synergy Software, Reading PA USA).

Crystallization

Throughout the crystallization studies, unless mentioned otherwise, the crystallization buffer consisted of 20% (w/v) polyethylene glycol 4000 (PEG 4000), 5% (v/v) ethylene glycol, 0.2 M $ZnCl_2$ and 0.1 M imidazole (pH 7.02). The cryoprotectant buffer contained 25% (w/v) PEG 4000, 24% (v/v) ethylene glycol, 0.2 M $ZnCl_2$ and 0.1 M imidazole, (pH 7.02).

Crystals of oxidized G20c$_3$

Crystals of oxidized G20c_3 were grown at 22 °C in hanging drops of equal volumes of the crystallization buffer and a freshly purified protein stock solution having a concentration of 6 mg/ml (0.5 mM). Generally, crystals formed within four days and matured over a period of two to three weeks. The crystals were soaked in cryoprotectant buffer for 30 min and were flash-frozen in liquid N_2.

Crystals of oxidized G20c$_3$ complexed with molybdate

Crystals of a cytochrome/molybdate complex were obtained by soaking oxidized crystals in crystallization buffer comprised of 20% (w/v) PEG 4000, 5% (v/v) ethylene glycol, 10 mM Na_2MoO_4 and 0.1 M imidazole (pH 7.02) for 20 min. Subsequent to this treatment, crystals were soaked for 2 min in cryoprotecting buffer containing 20% (w/v) PEG 4000, 25% (v/v) ethylene glycol, 10 mM Na_2MoO_4 and 0.1 M imidazole (pH 7.02) and flash-frozen in liquid N_2.

X-ray diffraction data collection

Data for an oxidized G20c_3 crystal (PDB accession code 2A3M) were collected at beamline 19ID of the Structural Biology Center at the Advanced Photon Source. The data for the molybdate-bound (2A3P) crystals were collected on an R-Axis IV image plate detector mounted on a Rigaku rotating anode generator. All data collections were performed using cryocooled crystals, and the data were processed with HKL.[55] Data collection statistics are summarized in Table 2.

Structure determination and refinement

The structure of oxidized G20c_3 was determined by the molecular replacement (MR) method using AMoRe[56] as implemented in the CCP4 package.[57] The search model used for MR calculations was a poly-alanine form of the tetraheme cytochrome c_3 structure from *D. vulgaris* Hildenborough (DvHc_3, PDB code 2CTH). An anomalous difference Fourier map calculated from the MR phases had strong peaks at the expected postions of the four Fe ions, which verified the correctness of the MR solution. Assignment of the side-chains and manual model rebuilding was done using O.[58] The initial model was improved through several iterated cycles of manual model rebuilding in O followed by refinement in X-PLOR.[59] After the protein and heme parts of the model were completed, water molecules were added to the model with COOT and the structure was refined with REFMAC5.[60] The high quality of the maps allowed modeling of alternative side-chain conformations at residues Glu2, Ser23 and Ser25.

The oxidized structure, with water, heme molecules and alternative side-chain conformations removed, served as the starting point for refinements of the molybdate-bound structure. Model building for this structure was done with COOT and refinement was done with REFMAC5. A common set of test reflections (10%) was used for refinement of both structures. An anomalous difference Fourier map calculated from the molybdate data set and phases from a partially refined model featured a very strong peak (17 σ) near a propionate group of heme IV (Figure 4). This feature was the highest peak of the map and it was presumed to represent a molybdate ion. For reference, the map had peaks of 8–9 σ at the locations of the heme Fe ions. Refinement statistics for both structures are summarized in Table 2.

Conserved solvent analysis

Conserved solvent sites of the TpI-*c*3 family were identified and analyzed using the pseudo-electron density map superposition method of Bottoms *et al.*[61] Briefly, the secondary structure matching (SSM) web server[42] was used to assemble a non-redundant set of TpI-*c*3 structures using our oxidized G20c_3 structure (2A3M) as the query and the default parameters of SSM. The resulting data set consisted of the following structures: 1I77 from *D. desulfuricans* Essex 6,[19] 1J0P from *D. vulgaris* Miyazaki,[62] 1WAD from *D. gigas*,[18] 2A3M (this work), 2CTH refinement of *D. vulgaris* Hildenborough,[19] and 3CYR refinement from *D. desulfuricans* ATCC 27774.[19] The high-resolution limits of these structures are in the range 0.91–1.95 Å. The pairwise amino acid sequence identities for the set span the range 39–86%, with an average of 52% and standard deviation of 16%. The structures were superimposed onto 2A3M and the superimposed set (including 2A3M) was used to calculate a pseudo-electron density map, which represents the distribution of water molecules in the superimposed structures. Clusters of water molecules were defined as being within 2 Å of a peak of the map. Water molecules in a given cluster with at least one conserved interaction with a polar atom of the protein (3.2 Å cutoff) were considered to be structurally equivalent.

Acknowledgements

We thank the personnel of APS beamline 19-ID for assistance with data collection, especially Stephan L. Ginell and Younchang Kim. We thank Peter Tipton for advice on stopped-flow fast kinetic analysis. Use of the Argonne National Laboratory Structural Biology Center beamlines at the Advanced Photon Source was supported by the U. S. Department of Energy, Office of Energy Research, under Contract no. W-31-109-ENG-38. This work was supported by the U.S. Department of Energy (DOE) Biological and Environmental Research Program (BER) and the DOE Natural and Accelerated Bioremediation Research Program (NABIR) Grant nos DE-FG02-01ER63155 and DE-FG02-87ER13713 and the Missouri Agricultural Experiment Station. C.A.B. was supported by a National Library of Medicine fellowship.

References

1. Lovley, D. R. (1993). Dissimilatory metal reduction. *Annu. Rev. Microbiol.* **47**, 263–290.
2. Lloyd, J. R., Nolting, H.-F., Sole, V. A., Bosecker, K. & Macaskie, L. E. (1998). Technetium reduction and precipitation by sulfate-reducing bacteria. *Geomicrobiol. J.* **15**, 45–58.
3. Lovley, D. R. & Phillips, E. J. P. (1992). Reduction of uranium by *Desulfovibrio desulfuricans*. *Appl. Environ. Microbiol.* **58**, 850–856.
4. Lovley, D. R. & Phillips, E. J. P. (1992). Bioremediation of uranium contamination with enzymatic uranium reduction. *Environ. Sci. Technol.* **26**, 2228–2234.
5. Coutinho, I. B. & Xavier, A. V. (1994). Tetraheme cytochromes. *Methods Enzymol.* **243**, 119–140.
6. Yagi, T. H. & Tamiya, M. N. (1968). Purification and properties of hydrogenases of different origins. *Biochim. Biophys. Acta*, **153**, 699–705.
7. Louro, R. O., Catarino, T., LeGall, J. & Xavier, A. V. (1997). Redox-Bohr effect in electron/proton energy transduction: cytochrome c_3 coupled to hydrogenase works as a 'proton thruster' in *Desulfovibrio vulgaris*. *J. Biol. Inorg. Chem.* **2**, 488–491.
8. Lovley, D. R., Widman, P. K., Woodward, J. C. & Phillips, E. J. P. (1993). Reduction of uranium by cytochrome c_3 of *Desulfovibrio vulgaris*. *Appl. Environ. Microbiol.* **59**, 3572–3576.
9. Payne, R. B., Gentry, D. N., Giles, B. J., Casalot, L. & Wall, J. D. (2002). Uranium reduction by *Desulfovibrio desulfuricans* strain G20 and a cytochrome c_3 mutant. *Appl. Environ. Microbiol.* **68**, 3129–3132.
10. Valente, F. M. A., Saraiva, L. M., LeGall, J., Xavier, A. V., Teixeira, M. & Pereira, I. A. C. (2001). A membrane-bound cytochrome c_3: a type II cytochrome c_3 from *Desulfovibrio vulgaris* Hildenborough. *ChemBioChem*, **2**, 895–905.
11. ElAntak, L., Dolla, A., Durand, M.-C., Bianco, P. & Guerlesquin, F. (2005). Role of the tetrahemic subunit in *Desulfovibrio vulgaris* Hildenborough formate dehydrogenase. *Biochemistry*, **44**, 14828–14834.
12. Bento, I., Matias, P. M., Baptista, A. M., da Costa, P. N., van Dongen, W. M. A. M., Saraiva, L. M. *et al*. (2004). Molecular basis for redox-Bohr and co-operative effects in cytochrome c_3 from *Desulfovibrio desulfuricans* ATCC 27774: crystallographic and modeling studies of oxidized and reduced high-resolution structures at pH 7.6. *Proteins: Struct. Funct. Bioinformatics*, **54**, 135–152.
13. Gunner, M. R., Alexov, E., Torres, E. & Lipovaca, S. (1997). The importance of the protein in controlling the electrochemistry of heme metalloproteins: methods of calculation and analysis. *J. Biol. Inorg. Chem.* **2**, 126–134.
14. Caffrey, M. S., Daldal, F., Holden, H. M. & Cusanovich, M. A. (1991). Importance of a conserved hydrogen-bonding network in cytochromes *c* to their redox potentials and stabilities. *Biochemistry*, **30**, 4119–4125.
15. Goodin, D. B. & McRee, D. E. (1993). The Asp-His-iron triad of cytochrome *c* peroxidase controls the reduction potential electronic structure, and coupling of the tryptophan free radical to the heme. *Biochemistry*, **32**, 3313–3324.
16. Higuchi, Y., Kusunoki, M., Matsura, Y., Yasuoka, N. & Kakudo, M. (1984). Refined structure of cytochrome c_3 at 1.8 Å resolution. *J. Mol. Biol.* **172**, 109–139.
17. Czjzek, M., Payan, F., Guerlesquin, F., Bruschi, M. & Haser, R. (1994). Crystal structure of cytochrome c_3 from *Desulfovibrio desulfuricans* Norway at 1.7 Å resolution. *J. Mol. Biol.* **243**, 653–667.
18. Matias, P. M., Morais, J., Coelho, R., Carrondo, M. A., Wilson, K., Dauter, Z. & Sieker, L. (1996). Cytochrome c_3 from *Desulfovibrio gigas*: crystal structure at 1.8 Å resolution and evidence for a specific calcium-binding site. *Protein Sci.* **5**, 1342–1354.
19. Simões, P., Matias, P. M., Morais, J., Wilson, K., Dauter, Z. & Carrondo, M. A. (1998). Refinement of the three-dimensional structures of cytochrome c_3 from *Desulfovibrio vulgaris* Hildenborough at 1.67 Å resolution and from *Desulfovibrio desulfuricans* ATCC 27774 at 1.6 Å resolution. *Inorg. Chim. Acta*, **273**, 213–224.
20. Nørager, S., Legrand, P., Pieulle, L., Hatchikian, C. & Roth, M. (1999). Crystal structure of the oxidized and reduced cytochrome c_3 from *Desulfovibrio africanus*. *J. Mol. Biol.* **290**, 881–902.
21. Einsle, O., Foerster, S., Mann, K., Fritz, G., Messerschmidt, A. & Kroneck, P. M. H. (2001). Spectroscopic investigation and determination of reactivity and structure of the tetraheme cytochrome c_3 from *Desulfovibrio desulfuricans* Essex 6. *Eur. J. Biochem.* **268**, 3028–3035.
22. Santos, H., Moura, J. J. G., Moura, I., LeGall, J. & Xavier, A. V. (1984). NMR studies of electron transfer mechanisms in a protein with interacting redox centers: *Desulfovibrio gigas* cytochrome c_3. *Eur. J. Biochem.* **141**, 283–296.
23. Messias, A. C., Kastrau, D. H. W., Costa, H. S., LeGall, J., Turner, D. L., Santos, H. & Xavier, A. V. (1998). Solution structure of *Desulfovibrio vulgaris* (Hildenborough) ferrocytochrome c_3: structural basis for functional cooperativity. *J. Mol. Biol.* **281**, 719–739.
24. Brennan, L., Turner, D. L., Messias, A. C., Teodoro, M. L., LeGall, J., Santos, H. & Xavier, A. V. (2000). Structural basis for the network of functional cooperativities in cytochrome c_3 from *Desulfovibrio gigas*: solution structures of the oxidized and reduced states. *J. Mol. Biol.* **298**, 61–82.
25. Harada, E., Fukuoka, Y., Ohmura, T., Fukunishi, A., Kawai, G., Fujiwara, T. & Akutsu, H. (2002). Redox-coupled conformational alternations in cytochrome c_3 from *Desulfovibrio vulgaris* Miyazaki F on the basis of its reduced solution structure. *J. Mol. Biol.* **319**, 767–778.

26. ElAntak, L., Morelli, X., Bornet, O., Hatchikian, C., Czjzek, M., Dolla, A. & Guerlesquin, F. (2003). The cytochrome c_3 -[Fe]-hydrogenase electron-transfer complex: structural model by NMR restrained docking. *FEBS Letters*, **548**, 1–4.
27. Czjzek, M., ElAntak, L., Zamboni, V., Morelli, X., Dolla, A., Guerlesquin, F. & Bruschi, M. (2002). The crystal structure of the hexadeca-heme cytochrome Hmc and a structural model of its complex with cytochrome c_3. *Structure*, **10**, 1677–1686.
28. Moura, J. J., Xavier, A. V., Bruschi, M. & LeGall, J. (1977). NMR characterization of three forms of ferredoxin from *Desulphovibrio gigas*, a sulphate reducer. *Biochim. Biophys. Acta*, **459**, 278–289.
29. Bell, G. R., Lee, J. P., Peck, H. D., Jr & LeGall, J. (1978). Reactivity of *Desulfovibrio gigas* hydrogenase towards artificial and natural electron donors. *Biochimie*, **60**, 315–320.
30. Mus-Veteau, I., Chottard, G., Lexa, D., Guerlesquin, F. & Bruschi, M. (1992). Cytochrome c_3-heteropolytungstate complex: a model for the interaction of the tetraheme cytochrome with its redox partners, ferredoxin and rubredoxin. *Biochim. Biophys. Acta*, **1102**, 353–359.
31. Palma, P. N., Moura, I., LeGall, J., Van Beeumen, J., Wampler, J. & Moura, J. J. (1994). Evidence for a ternary complex formed between flavodoxin and cytochrome c_3: 1H-NMR and molecular modeling studies. *Biochemistry*, **33**, 6394–6407.
32. Payne, R. B., Casalot, L., Rivere, T., Terry, J. H. & Wall, J. D. (2004). Interaction between uranium and the cytochrome c_3 of *Desulfovibrio desulfuricans* strain G20. *Arch. Microbiol.* **181**, 398–406.
33. Assfalg, M., Bertini, I., Bruschi, M., Michel, C. & Turano, P. (2002). The metal reductase activity of some multiheme cytochromes *c*: NMR structural characterization of the reduction of chromium(VI) to chromium(III) by cytochrome c_7. *Proc. Natl Acad. Sci. USA*, **99**, 9750–9754.
34. Michel, C., Brugna, M., Aubert, C., Bernadac, A. & Bruschi, M. (2001). Enzymatic reduction of chromate: comparative studies using sulfate-reducing bacteria. Key role of polyheme cytochromes *c* and hydrogenases. *Appl. Microbiol. Biotechnol.* **55**, 95–100.
35. Myer, Y. P. & Pande, A. (1978). Circular dichroism studies of hemoproteins and heme models. In *The Porphyrins* (Dolphins, D., ed.), pp. 271–322, Academic Press, New York.
36. Manning, M. (1989). Underlying assumptions in the estimation of secondary structure content in proteins by circular dichroism spectroscopy- a critical review. *J. Pharm. Biomed. Anal.* **7**, 1103–1119.
37. Dolla, A., Florens, L., Bruschi, M., Dudich, I. V. & Makarov, A. A. (1995). Drastic influence of a single heme axial ligand replacement on the thermostability of cytochrome c_3. *Biochem. Biophys. Res. Commun.* **211**, 742–747.
38. John, D. M. & Weeks, K. M. (2000). van't Hoff enthalpies without baselines. *Protein Sci.* **9**, 1416–1419.
39. Uchiyama, S., Ohshima, A., Nakamura, S., Hasegawa, J., Terui, N., Takayama, Y. *et al*. (2004). Complete thermal-unfolding profiles of oxidized and reduced cytochromes *c*. *J. Am. Chem. Soc.* **126**, 14684–14685.
40. Johnson, K. A. (1992). Transient-state kinetic analysis of enzyme reaction pathways. In *The Enzymes* (Sigman, D. S., ed.), vol. 20, pp. 1–61, Academic Press, San Diego.
41. Matias, P. M., Frazao, C., Morais, J., Coll, M. & Carrondo, A. (1993). Structure analysis of cytochrome c_3 from *Desulfovibrio vulgaris* Hildenborough at 1.9 Å resolution. *J. Mol. Biol.* **234**, 680–699.
42. Krissinel, E. & Henrick, K. (2004). Secondary-structure matching (SSM), a new tool for fast protein structure alignment in three dimensions. *Acta Crystallog. sect. D*, **60**, 2256–2268.
43. Salgueiro, C. A., Morgado, L., Fonseca, B., Lamosa, P., Catarino, T., Turner, D. L. & Louro, R. O. (2005). Binding of ligands originates small perturbations on the microscopic thermodynamic properties of a multicentre redox protein. *FEBS J.* **272**, 2251–2260.
44. Salgueiro, C. A., da Costa, P. N., Turner, D. L., Messias, A. C., van Dongen, W. M. A. M., Saraiva, L. M. & Xavier, A. V. (2001). Effect of hydrogen-bond networks in controlling reduction potentials in *Desulfovibrio vulgaris* (Hildenborough) cytochrome c_3 probed by site-specific mutagenesis. *Biochemistry*, **40**, 9709–9716.
45. Aragao, D., Frazao, C., Sieker, L., Sheldrick, G. M., LeGall, J. & Carrondo, M. A. (2003). Structure of dimeric cytochrome c_3 from *Desulfovibrio gigas* at 1.2 Å resolution. *Acta Crystallog. sect. D*, **59**, 644–653.
46. Aubert, C., Giudici-Orticoni, M. T., Czjzek, M., Haser, R., Bruschi, M. & Dolla, A. (1998). Structural and kinetic studies of the Y73E mutant of octaheme cytochrome c_3 (Mr = 26 000) from *Desulfovibrio desulfuricans* Norway. *Biochemistry*, **37**, 2120–2130.
47. Meyer, E. (1992). Internal water molecules and H-bonding in biological macromolecules: a review of structural features with functional implications. *Protein Sci.* **1**, 1543–1562.
48. Weimer, P. J., Van Kavelaar, M. J., Michel, C. B. & Ng, T. K. (1988). Effect of phosphate on the corrosion of carbon steel and on the composition of corrosion products in two-stage continuous cultures of *Desulfovibrio desulfuricans*. *Appl. Environ. Microbiol.* **54**, 386–396.
49. Wall, J. D., Rapp-Giles, B. J. & Rousset, M. (1993). Characterization of a small plasmid from *Desulfovibrio desulfuricans* and its use for shuttle vector construction. *J. Bacteriol.* **175**, 4121–4128.
50. Rapp-Giles, B. J., Casalot, L., English, R. S., Ringbauer, J. r., J, A., Dolla, A. & Wall, J. D. (2000). Cytochrome c_3 mutants of *Desulfovibrio desulfuricans*. *Appl. Environ. Microbiol.* **66**, 671–677.
51. van der Westen, H. M., Mayhew, S. G. & Veeger, C. (1978). Separation of hydrogenase from intact cells of *Desulfovibrio vulgaris*. *FEBS Letters*, **86**, 122–126.
52. Fournier, M., Zhang, Y., Wildschut, J. D., Dolla, A., Voordouw, J. K., Schriemer, D. C. & Voordouw, G. (2003). Function of oxygen resistance proteins in the anaerobic, sulfate-reducing bacterium *Desulfovibrio vulgaris* Hildenborough. *J. Bacteriol.* **185**, 71–79.
53. Thomas, P., Ryan, D. & Levin, W. (1976). An improved staining procedure for the detection of the peroxidase activity of cytochrome P_{450} on sodium dodecyl sulfate polyacrylamide gels. *Anal. Biochem.* **75**, 168–175.
54. Bradford, M. M. (1976). A rapid and sensitive method for the quantitation of microgram quantities of protein utilizing the principle of protein–dye binding. *Anal. Biochem.* **72**, 248–254.
55. Otwinowski, Z. & Minor, W. (1997). Processing of X-ray diffraction data collected in oscillation mode. *Methods Enzymol.* **276**, 307–326.
56. Navaza, J. (2001). Implementation of molecular replacement in AMoRe. *Acta Crystallog. sect. A*, **57**, 1367–1372.
57. Collaborative Computational Project, Number 4. (1994). The CCP4 suite: programs for protein crystallography. *Acta Crystallog. sect. D*, **50**, 760–763.

58. Jones, T. A., Zou, J. Y., Cowan, S. W. & Kjeldgaard, M. (1991). Improved methods for the building of protein models in electron density maps and the location of errors in these models. *Acta Crystallog. sect. A*, **47**, 110–119.
59. Brünger, A. T. (1996). *X-PLOR: a System for X-ray Crystallography and NMR, version 3.1*, Yale University, CT, USA.
60. Winn, M. D., Murshudov, G. N. & Papiz, M. Z. (2003). Macromolecular TLS refinement in REFMAC at moderate resolutions. *Methods Enzymol.* **374**, 300–321.
61. Bottoms, C. A., White, T. A. & Tanner, J. J. (2006). Exploring structurally conserved solvent sites in protein families. *Proteins: Struct. Funct. Bioinformatics*, in the press.
62. Ozawa, K., Takayama, Y., Yasukawa, F., Ohmura, T., Cusanovich, M. A., Tomimoto, Y. *et al*. (2003). Role of the aromatic ring of Tyr43 in tetraheme cytochrome c_3 from *Desulfovibrio vulgaris* Miyazaki F. *Biophys. J.* **85**, 3367–3374.
63. Engh, R. A. & Huber, R. (1991). Accurate bond and angle parameters for x-ray protein structure refinement. *Acta Crystallog. sect. A*, **47**, 392–400.
64. Laskowski, R. A., MacArthur, M. W., Moss, D. S. & Thornton, J. M. (1993). PROCHECK: a program to check the stereochemical quality of protein structures. *J. Appl. Crystallog.* **26**, 283–291.

Edited by M. Guss

(Received 7 December 2005; received in revised form 1 March 2006; accepted 4 March 2006)
Available online 23 March 2006